J Elast (2017) 129:257–281
DOI 10.1007/s10659-017-9631-8

A Comparison of Phenomenologic Growth Laws for Myocardial Hypertrophy

Colleen M. Witzenburg[1] · Jeffrey W. Holmes[1,2,3]

Received: 3 June 2016 / Published online: 1 March 2017

Abstract The heart grows in response to changes in hemodynamic loading during normal development and in response to valve disease, hypertension, and other pathologies. In general, a left ventricle subjected to increased afterload (pressure overloading) exhibits concentric growth characterized by thickening of individual myocytes and the heart wall, while one experiencing increased preload (volume overloading) exhibits eccentric growth characterized by lengthening of myocytes and dilation of the cavity. Predictive models of cardiac growth could be important tools in evaluating treatments, guiding clinical decision making, and designing novel therapies for a range of diseases. Thus, in the past 20 years there has been considerable effort to simulate growth within the left ventricle. While a number of published equations or systems of equations (often termed "growth laws") can capture some aspects of experimentally observed growth patterns, no direct comparisons of the various published models have been performed. Here we examine eight of these laws and compare them in a simple test-bed in which we imposed stretches measured during *in vivo* pressure and volume overload. Laws were compared based on their ability to predict experimentally measured patterns of growth in the myocardial fiber and radial directions as well as the ratio of fiber-to-radial growth. Three of the eight laws were able to reproduce most key aspects of growth following both pressure and volume overload. Although these three growth laws utilized different approaches to predict hypertrophy, they all employed multiple inputs that were weakly correlated during *in vivo* overload and therefore provided independent information about mechanics.

Keywords Overload · Remodeling · Adaptation · Cardiac mechanics · Ventricle · Computer model

Electronic supplementary material The online version of this article (doi:10.1007/s10659-017-9631-8) contains supplementary material, which is available to authorized users.

✉ J.W. Holmes
holmes@virginia.edu

1 Department of Biomedical Engineering, University of Virginia, Charlottesville, VA, USA

2 Department of Medicine, University of Virginia, Charlottesville, VA, USA

3 Robert M. Berne Cardiovascular Research Center, University of Virginia, Charlottesville, VA, USA

Mathematics Subject Classification 74D10 · 74E99 · 74L15

1 Introduction

Hypertrophy of the adult left ventricle (LV) is frequently described in terms of two prototypical patterns: concentric and eccentric hypertrophy. Experimentally, pressure overloading of the LV leads to concentric hypertrophy (thickening of individual myocytes and the heart wall), whereas volume overloading of the LV leads to eccentric hypertrophy (lengthening of myocytes and dilation of the cavity) [1, 2]. While some conditions such as hypertension are clearly associated with pressure overloading and concentric hypertrophy and others such as mitral regurgitation are clearly associated with volume overloading and eccentric hypertrophy, many involve some combination of the two. Myocardial infarction, congenital heart defects, some heart valve diseases, pregnancy, and athletic training all induce hypertrophy falling along a spectrum ranging from concentric to eccentric growth. Thus predicting growth and remodeling in these settings requires models that capture responses across this entire spectrum. Since hypertrophy is often progressive, the most pertinent clinical questions surrounding disorders tend to be prognostic: even simply anticipating the rate of progression can be essential when planning treatment. Thus, though the underlying mechanisms responsible for hypertrophy remain elusive [3, 4], phenomenologic models have the potential to provide insight into the development of hypertrophy and guide clinical decision making, in addition to aiding in the design of device-based therapies to slow or reverse remodeling.

Rodriguez et al. [5] presented a general theory for volumetric growth. Together with a set of equations (usually termed a "growth law") that specify how rapidly a region of the heart will grow in any given situation, this framework can predict how cardiac dimensions, residual stresses, and the response to repeated cyclic loading will evolve over time. Because changes in mechanical loading of the heart clearly induce growth and remodeling, many growth laws utilize measures of local mechanics to drive predicted growth. However, there has been considerable debate concerning which specific growth stimuli are actually sensed by the cells in the heart, or (perhaps more practically) which metrics provide the best basis for formulating growth laws. Grossman et al. [6] found that estimated wall stresses in patients with pressure overload were not different from those in normal subjects, and proposed that peak systolic stress may act as a stimulus for concentric hypertrophy, eventually normalizing the initial increases in wall stress due to elevated pressures. Emery and Omens [7] concluded that end-diastolic fiber strain was normalized during volume overload, making it a likely candidate stimulus for eccentric hypertrophy. Holmes [8] investigated potential stimuli during volume overload more systematically and concluded that volume amplitude or related metrics such as ejection strain could provide a basis for distinguishing between pressure and volume overload. Due to the uncertainty surrounding both the underlying biology and the predictive value of the many available potential stimuli, selecting or formulating a growth law is challenging.

A number of growth laws have been proposed and demonstrated to fit aspects of the growth response following pressure and/or volume overloading. It is difficult to compare published laws from various studies, however, since each study uses a different left ventricular geometry, passive constitutive relation, active model of contraction, and set of circulation conditions. Here, we compared eight different growth laws directly. We employed published reports to identify the changes in stretch that occur *in vivo* during acute pressure and volume overloading. Then, we applied these stretches in a simple test-bed and predicted growth using each of the eight growth laws. Finally, we compared features of the growth predicted by

each law to reported measurements of myocyte dimensions following pressure or volume overload to assess the ability of each law to capture experimentally observed trends.

2 Methods

2.1 Growth Framework

We performed a direct comparison of several published growth laws (Table 1). All of these growth laws assumed constant density of added or subtracted myocardium (so that growth manifests as a change in volume) and utilized the theoretical framework of Rodriguez et al. [5]. In this framework, material is added or removed through a growth deformation, F_g, changing the local stress-free configuration. The overall deformation is given by

$$F_{eg} = F_e F_g, \tag{1}$$

where the growth deformation, F_g, maps the original reference state to an intermediary unstressed (and potentially incompatible) grown state. The elastic deformation, F_e, then maps the intermediary state into the intact, loaded state. Only the elastic deformation contributes to stress.

As outlined below, we prescribed diastolic and systolic circumferential and longitudinal stretches typical of normal hearts or of hearts subjected to hemodynamic overload, then used the various growth laws to predict the resulting growth. In the context of Eq. (1), this was implemented by prescribing F_{eg} values, computing F_g for a single growth step using one of the growth laws, computing the new diastolic and systolic elastic deformations ($F_e = F_{eg} F_g^{-1}$), and iterating until steady-state was reached or a pre-specified growth limit was exceeded. In order to visually compare the responses of the various growth laws detailed below, Figure S1 plots the growth rate of each law as elastic fiber or crossfiber stretch is varied over the range explored in this study.

2.2 Growth Laws

2.2.1 A Model for Stress-Induced Growth in the Developing Heart: L&T

Lin and Taber [9] considered how embryonic growth is affected by mechanical loading. While they acknowledged that pre-natal growth is dominated by hyperplasia and post-natal growth by hypertrophy, they argued that the basic patterns of growth in which the ventricle increases in size in response to increases in pressure and volume are similar. They created a stress-based growth law in which they approximated the LV as a cylindrical thick-walled pressure vessel, simulated passive inflation during diastole, and prescribed growth based on end-diastolic stresses. The fiber direction (f) was assumed to be circumferential and the cross-fiber direction (c) to be parallel to the cylinder axis, with both axes perpendicular to the radial direction (r). Their growth law took the form:

$$F_{g,j}^{i+1} = \frac{F_{g,j}^{i}}{[1 + F_{g,j}^{i} * - \sum_k D_{jk}(\sigma_k - \sigma_{set,k})]}, \tag{2}$$

where $(k, j) = (f, c, r)$, D is a matrix of growth rate coefficients determined by fitting data from embryonic chick left ventricles in both normal and pressure-overloaded states, σ is the Cauchy stress at end diastole, and σ_{set} is the end-diastolic Cauchy stress at growth equilibrium. The superscript i indicates the growth time step. Lin and Taber originally chose $\sigma_{set} = 0$ for all three directions; as explained below, we chose new setpoints to achieve zero growth in all directions under baseline loading conditions.

Table 1 Growth laws compared and modified input set-points

Law	Geometry	Material description		Input parameters	Original set-point	Modified set-point
		Passive	Active			
L&T	Thick walled cylinder	compressible isotropic Fung-type exponential	none	end-diastolic stress in the fiber, cross-fiber, and radial directions	$\sigma_{set,f} = 0$ mmHg $\sigma_{set,c} = 0$ mmHg $\sigma_{set,r} = 0$ mmHg	$\sigma_{set,f} = 1.92$ mmHg $\sigma_{set,c} = 1.92$ mmHg $\sigma_{set,r} = -1.38$ mmHg
LT2	Thick walled cylinder	linear elastic	linear elastic	diastolic and systolic stress in the fiber direction	$\sigma_{set,a} = 30$ kPa $\sigma_{set,p} = 3$ kPa	$\sigma_{set,a} = 1170$ kPa $\sigma_{set,p} = 88$ kPa
KFR	Truncated ellipsoid	slightly compressible anisotropic exponential	none	end-diastolic fiber strain	$s_{hom} = 0.13$	$s_{hom} = 0.44$
KUR	Truncated ellipsoid	slightly compressible anisotropic exponential	none	end-diastolic fiber strain	$s_{hom} = 0.13$	$s_{hom} = 0.44$
GEG	Truncated ellipsoid	compressible isotropic neo-Hookean	none	end-diastolic fiber strain	$F_{g,f,max} = 1.50$ $\lambda^{crit} = 1.01$	$F_{g,f,max} = 1.50$ $\lambda^{crit} = 1.44$
GCG	Truncated ellipsoid	compressible isotropic neo-Hookean	none	first invariant of the Mandel stress at end systole	$F_{g,c,max} = 3.00$ $p^{crit} = 0.012$ Mpa	$F_{g,c,max} = 3.00$ $p^{crit} = 0.053$ Mpa
ART	Chamber	compressible anisotropic exponential	Hill-type model	maximum and minimum sarcomere lengths	$L_{s,max,adapt} = 2.30$ µm $L_{s,min,adapt} = 1.75$ µm	$L_{s,max,adapt} = 2.07$ µm $L_{s,min,adapt} = 1.61$ µm
KOM	Finite element model of canine left ventricle	slightly compressible transversely isotropic	Hill-type model	maximum fiber strain and the minimum maximum principal cross-section strain	$E_{f,set} =$ not given $E_{cross,set} =$ not given	$E_{f,set} = 0.537$ $E_{cross,set} = 0.124$

2.2.2 *Biomechanical Growth Laws for Muscle Tissue: LT2*

Taber [10] also considered muscle development more generally, creating growth laws for skeletal muscle, heart muscle, and arteries. In this case the full range of post-natal growth, from birth to maturity, was simulated. For heart growth, the LV was again approximated as a cylindrical thick-walled pressure vessel. Both passive and active stresses were considered, and growth was determined based on stress in the circumferential direction. Thus, in L&T all directions were considered (circumferential, radial, and longitudinal), but only at end-diastole, whereas in LT2 stress both at end-diastole and end-systole was considered, but only in the circumferential direction. Here again, the fiber direction (f) was assumed to be circumferential and the cross-fiber direction (c) to be parallel to the cylinder axis, with both axes perpendicular to the radial direction (r). The growth law took the form:

$$F_{g,r}^{i+1} = F_{g,r}^{i} * \left(\frac{1}{\overline{\overline{T}}_r} * \frac{1}{(\sigma_{\theta a0})_m} * \left[\sigma_{\theta a} - (\sigma_{\theta a0})_m \right] + 1 \right), \tag{3}$$

$$F_{g,f}^{i+1} = F_{g,f}^{i} * \left(\frac{1}{\overline{\overline{T}}_\theta} * \frac{1}{(\sigma_{\theta p0})_m} * \left[\sigma_{\theta p} - (\sigma_{\theta p0})_m \right] + 1 \right), \tag{4}$$

$$F_{g,c}^{i+1} = 1 \tag{5}$$

where $\overline{T}_r$ and $\overline{T}_\theta$ are normalized time constants and $(\sigma_{\theta a0})_m$ and $(\sigma_{\theta p0})_m$ are the active and passive fiber stresses at growth equilibrium. These equilibrium stresses were adjusted to achieve zero growth in all directions under baseline conditions.

2.2.3 *Computational Modeling of Volumetric Soft Tissue Growth: Application to the Cardiac Left Ventricle: KFR and KUR*

Like Lin and Taber, Kroon et al. [11] also simulated passive inflation during diastole, but used a finite-element truncated ellipsoidal model of the LV to simulate the response to volume overload rather than pressure overload, employing growth laws that depended on strain rather than stress. In the "fixed" reference configuration growth law (denoted KFR), the stress-free reference configuration remained constant throughout the simulation,

$$F_{g,j}^{i+1} = \left[\beta(\sqrt{2 * E_{ff} + 1} - 1 - s_{hom}) + 1 \right]^{\frac{1}{3}} F_{g,j}^{i}. \tag{6}$$

By contrast, their "updated" reference configuration growth law considered the possibility that turnover of tissue components might allow growth-induced residual stresses to relax over time. In this growth law (denoted KUR),

$$F_{g,j}^{i+1} = \left[\beta(\sqrt{2 * E_{ff} + 1} - 1 - s_{hom}) + 1 \right]^{\frac{1}{3}}. \tag{7}$$

In both laws, β is the product of the growth rate constant and the time interval, s_{hom} is the homeostatic end-diastolic myofiber strain, and E_{ff} is the elastic fiber strain at end diastole for growth time step i. In both cases growth was assumed to occur isotropically, thus $j = (f, c, r)$.

2.2.4 *A Multiscale Model for Eccentric and Concentric Cardiac Growth Through Sarcomerogenesis: GEG and GCG*

Göktepe et al. [12] used a finite-element model to simulate end diastole and end systole and proposed two different growth laws: one to simulate growth following volume overload

(eccentric hypertrophy) and one to simulate growth following pressure overload (concentric hypertrophy). For volume overload they utilized a strain-based growth law (here denoted GEG),

$$F_{g,f}^{i+1} = \frac{1}{\tau}\left[\frac{F_{g,f,max} - F_{g,f}^{i}}{F_{g,f,max} - 1}\right]^{\gamma} * \left[F_{e,f}^{i} - \lambda^{crit}\right] + F_{g,f}^{i} \quad \text{and} \tag{8}$$

$$F_{g,c}^{i+1} = F_{g,r}^{i+1} = 1, \tag{9}$$

where $F_{g,f,max}$ specifies the maximum fiber growth allowed and λ^{crit} is the homeostatic elastic fiber stretch. Note that growth is not permitted in the cross-fiber or radial directions. For pressure overload they utilized a stress-based growth law (denoted GCG),

$$F_{g,c}^{i+1} = \frac{1}{\tau}\left[\frac{F_{g,c,max} - F_{g,c}^{i}}{F_{g,c,max} - 1}\right]^{\gamma} * \left[\mathrm{tr}\left(M^{e}\right) - p^{crit}\right] + F_{g,c}^{i} \quad \text{and} \tag{10}$$

$$F_{g,f}^{i+1} = F_{g,r}^{i+1} = 1, \tag{11}$$

where $F_{g,c,max}$ specifies the maximum cross-fiber growth allowed, M^{e} is the Mandel stress (Cauchy stress weighted by the Jacobian) associated with the elastic deformation at end systole, and p^{crit} is the homeostatic value for the Mandel stress. Note that, in this case, growth is not permitted in the fiber or radial directions. In both laws, τ controls how much growth occurs per growth time step i and γ controls the shape of the growth-limiting function.

2.2.5 *Adaptation to Mechanical Load Determines Shape and Properties of Heart and Circulation: the CircAdapt Model: ART*

Arts et al. [13] combined an active model of sarcomere mechanics, analytic expressions relating fiber stretch and stress to cavity pressures and volumes, and a circuit model of the circulation to simulate the full cardiac cycle before and during pressure overload. They proposed a set of growth laws in which the ratio of maximum to minimum fiber stretch determined fiber growth, while a more complicated function of maximum and minimum fiber stretch determined radial growth:

$$F_{g,f}^{i+1} = \frac{\max(F_{e,f}^{i})/\min(F_{e,f}^{i})}{L_{s,max,adapt}/L_{s,min,adapt}} F_{g,f}^{i}, \tag{12}$$

$$F_{g,r}^{i+1} = F_{g,r}^{i}\sqrt{\left(\frac{1+a}{1+ae^{b(L_{s,max,adapt} - L_{s,0}^{i} * \max(F_{e,f}^{i}))}}\right) * \left(\frac{L_{s,max,adapt}/L_{s,min,adapt}}{\max(F_{e,f}^{i})/\min(F_{e,f}^{i})}\right)}, \tag{13}$$

$$L_{s,0}^{i+1} = L_{s,0}^{i}\left(\frac{L_{s,max,adapt}/L_{s,min,adapt}}{\max(F_{e,f}^{i})/\min(F_{e,f}^{i})}\right), \quad \text{and} \tag{14}$$

$$F_{g,c}^{i+1} = F_{g,r}^{i+1}, \tag{15}$$

where $L_{s,max,adapt}$ is the homeostatic set point for sarcomere length at the beginning of ejection, $L_{s,min,adapt}$ is the homeostatic set point for sarcomere length at the end of ejection, and a and b control the sensitivity to stretch. The value specified for the initial reference sarcomere length, $L_{s,0}^{1}$, did not affect the long-term behavior of this law, because $L_{s,0}^{i}$ changes with each growth time step i.

2.2.6 *A Single Strain-Based Growth Law Predicts Concentric and Eccentric Cardiac Growth During Pressure and Volume Overload: KOM*

Finally, Kerckhoffs et al. [14] proposed a single law consisting of a pair of sigmoidal strain-based equations to model the response to both pressure and volume overload. Similar to Arts et al. [13], they included a Hill-type model to simulate myocyte contraction and coupled their LV model to a model of the circulatory system to determine loading conditions for the ventricles. They did not allow the circulation parameters to change with growth, however, instead prescribing cardiac output. The stimuli for myocyte growth,

$$s_l = \max(E_{ff}) - E_{f,set} \quad \text{and} \tag{16}$$

$$s_t = \min\left(\frac{E_{cc}+E_{rr}}{2} + \sqrt{\left(\frac{E_{cc}-E_{rr}}{2}\right)^2 + E_{cr}^2}\right) - E_{cross,set}, \tag{17}$$

are dependent on the elastic fiber strain, E_{ff}, cross-fiber strain, E_{cc}, radial strain E_{rr}, and cross-fiber radial shear, E_{cr}. $E_{f,set}$ is the strain set-point at which no axial fiber growth occurs and $E_{cross,set}$ is the strain set-point at which no cross-fiber or radial growth occurs. Growth in the fiber direction is determined by

$$F_{g,f}^{i+1} = \begin{cases} F_{g,f}^{i} * \left[\frac{1}{1+e^{d_l*(F_{g,f}^{i}-F_{f,50})}} * \frac{a_l}{1+e^{-b_l*(s_l-s_{l,50})}} + 1\right] & s_l \geq 0 \\ F_{g,f}^{i} * \left[\frac{-a_l}{1+e^{b_l*(s_l+s_{l,50})}} + 1\right] & s_l < 0. \end{cases} \tag{18}$$

Growth is the same in the radial and cross-fiber directions and is determined by

$$F_{g,c}^{i+1} = F_{g,r}^{i+1} = \begin{cases} F_{g,c}^{i} * \left[\frac{1}{1+e^{d_t*(F_{g,c}^{i}-F_{c,50})}} * \frac{a_t}{1+e^{-b_t*(s_t-s_{t,50})}} + 1\right] & s_t \geq 0 \\ F_{g,c}^{i} * \left[\frac{-a_t}{1+e^{b_t*(s_t+s_{t,50})}} + 1\right] & s_t < 0. \end{cases} \tag{19}$$

Equations (15) and (16) prescribe sigmoidal functions such that maximum and minimum growth allowed within a single step is determined by the parameters a_l and a_t and there is a small nearly quiescent (low-growth) region near the setpoints specified by $s_{l,50}$, $s_{t,50}$, b_l, and b_t. When the stimulus is positive, i.e., $s_l \geq 0$ or $s_t \geq 0$, a limiting term is included to avoid cases of runaway growth.

2.3 Inputs to the Growth Laws: Control and Overloaded Stretches and Stresses

The LV has a complex fiber architecture in which myocardial fiber orientation changes as a function of both depth within the myocardial wall and distance from the base to the apex [15]. At the midwall, the fibers are aligned with the circumferential direction of the LV and the in-plane cross-fiber direction is aligned with the longitudinal axis of the LV. Measurements of circumferential and longitudinal strains during active contraction [16–19] and during passive inflation [20, 21] indicate that they are roughly equal. During the cardiac cycle, peak stretches in both the circumferential and longitudinal directions occur at end diastole, associated with significant radial thinning [8, 22–24]. Peak radial thickening occurs near end systole, when circumferential and longitudinal stretches are low. Thus, to provide a simple test-bed for comparing different growth laws, we simulated cyclic equibiaxial stretch of a thin slab of myocardium (Fig. 1) between prescribed end-diastolic and end-systolic stretches. Since the growth laws we tested were not sensitive to strain rate, we specified linear stretching/shortening between these extremes. We simulated changes in regional mechanics typical of pressure overload and volume overload by adjusting end-diastolic and

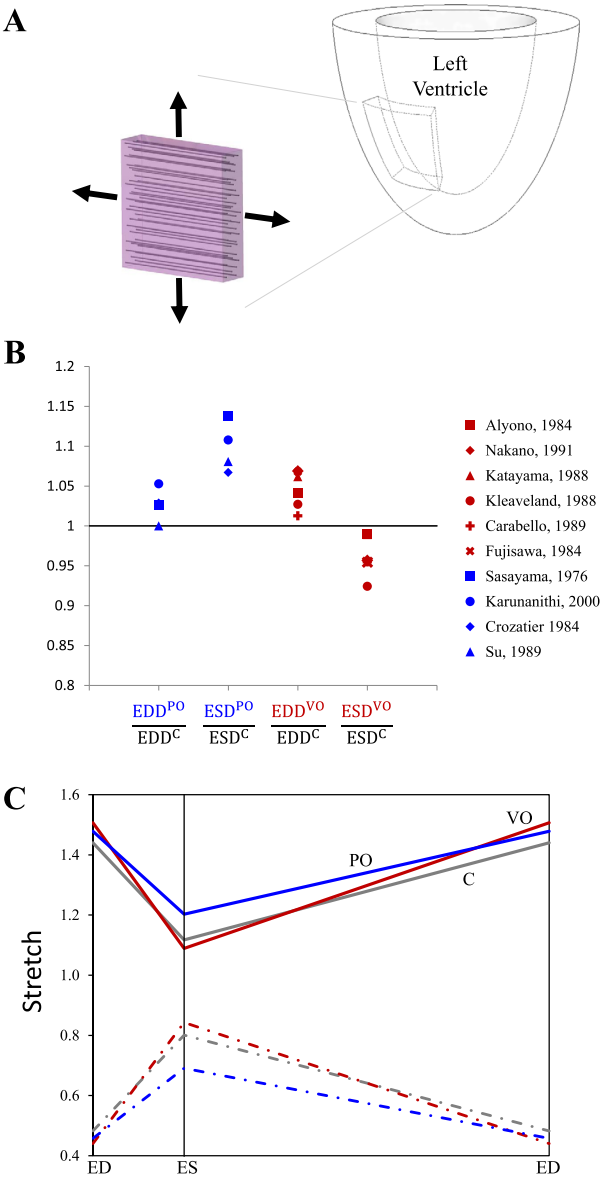

Fig. 1 (**A**) Schematic of mid-wall slab of left ventricular equatorial subjected to prescribed stretches in our simulations. (**B**) End-systolic and end-diastolic dimension ratios relative to control during acute pressure [34–37] and volume overload [28–33] studies. To avoid potentially confounding effects of growth normalizing the inciting stimulus, only studies that recorded dimensions prior to appreciable change in ventricular mass were considered. (**C**) Average stretch vs. cardiac cycle time for control (C), volume overload (VO), and pressure overload (PO) in reference to the stress-free configuration. ED signifies end diastole and ES signifies end systole. Equibiaxial loading was assumed, thus the fiber (*solid lines*) and cross-fiber (*dashed lines*) directions experienced the same stretch profile and radial (*dash-dot lines*) thinning was prescribed to maintain constant tissue volume

end-systolic stretches to match reported *in vivo* values, and observed the predicted growth responses.

The majority of the growth laws compared here predict growth based on elastic stretches or strains computed relative to a stress-free state. This stress-free state is a convenient reference when formulating models, but never occurs *in vivo*. We utilized end-diastolic pressure (EDP) and segment length data from Fomovsky et al. [25] to estimate end-diastolic circumferential stretch relative to the unloaded state in normal dogs. Fomovsky and colleagues recorded data during inferior vena cava occlusions, which produced a series of beats with gradually decreasing EDP. We plotted end-diastolic segment length as a function of ln(EDP)

and used a linear fit to estimate the intercept of this plot, corresponding to circumferential segment length at an EDP of 1 mmHg. We treated this segment length as an estimate of the unloaded length, and retained only the estimates with a coefficient of variation $< 5.0\%$. The average estimated end-diastolic circumferential stretch relative to the unloaded state in these 6 animals was 1.44 ± 0.10 (mean $\pm$ SEM, see Figure S2). However, unloaded hearts are not stress-free [26], and stretch ratios computed from unloaded segment lengths would not account for residual strains. Luckily, Rodriguez et al. [27] compared unloaded and stress-free sarcomere lengths in rats and found that while the transmural distribution of sarcomere lengths differed in these two states, the sarcomere length at the midwall was the same.

Next, we reviewed *in vivo* data to determine how stretch changes following the creation of experimental pressure and volume overload in dogs. To avoid potentially confounding effects of growth normalizing the inciting stimulus, only studies that recorded end-diastolic and end-systolic dimensions after the imposition of hemodynamic overload but prior to appreciable change in left ventricular mass were considered. Changes in left ventricular diameter or volume measured using angiography or sonomicrometry were used to estimate stretches during overload; where volumes were provided instead of dimensions, stretch ratios were estimated using volume ratio raised to the one-third power. Six studies induced experimental volume overload and reported changes in volumes within four days; two created aorto-caval fistulas [28, 29] and four induced mitral regurgitation [30–33]. In these studies, volume overload increased end-diastolic volume or diameter (end-diastolic stretch ratios of 1.05 ± 0.02 relative to control, mean $\pm$ SD, $p = 0.02$, Fig. 1B) and decreased end-systolic volume or diameter (end-systolic stretch ratios of 0.96 ± 0.02 relative to control, mean $\pm$ SD, $p = 0.04$). Four studies induced experimental pressure overload using ascending [34–36] or descending [37] aortic constriction and reported changes in left ventricular dimensions immediately. In these studies, pressure overload increased end-systolic volume or diameter (end-systolic stretch ratios of 1.10 ± 0.03 relative to control, mean $\pm$ SD, $p = 0.01$, Fig. 1B), while increases in end-diastolic volume or diameter were not significant (end-diastolic stretch ratios of 1.03 ± 0.02 relative to control, mean $\pm$ SD, $p = 0.09$).

The *in vivo* experimental stretch ratios were expressed relative to end diastole, rather than the unloaded configuration. Thus, for overload studies we computed end-diastolic stretches relative to the unloaded configuration by combining our estimate of control end-diastolic stretch relative to the unloaded state (λ_{ED}^{C}) with measurements of control (EDD^{C}), and overload (EDD^{O}) end-diastolic dimensions:

$$\lambda_{ED}^{O} = \lambda_{ED}^{C} * \frac{EDD^{O}}{EDD^{C}}. \tag{20}$$

Similarly, we computed end-systolic stretches for both control and overload states using the end-diastolic stretch relative to unloaded state and measurements of control and overload dimensions:

$$\lambda_{ES}^{C} = \lambda_{ED}^{C} * \frac{ESD^{C}}{EDD^{C}} \quad \text{or} \quad \lambda_{ES}^{O} = \lambda_{ED}^{O} * \frac{ESD^{O}}{EDD^{O}}. \tag{21}$$

The resulting stretch profiles used to simulate pressure and volume overload are shown in Fig. 1C. Control fiber and cross-fiber end-diastolic and end-systolic stretches were set to 1.44 and 1.12 at baseline, 1.48 and 1.20 to simulate pressure overload, and 1.51 and 1.09 to simulate volume overload. Myocardial tissue was assumed incompressible within each loading cycle. Thus, radial end-diastolic and end-systolic stretches were set to 0.48 and 0.80, 0.46 and 0.69, and 0.44 and 0.84, for control, pressure overload, and volume overload conditions, respectively. Three of the growth laws (L&T, LT2 and GCG) utilized stresses (rather than stretches or strains) as inputs; in these cases the stresses were computed from

the prescribed stretches using the constitutive equation provided in the original reference. Finally, to provide the most useful comparison of the predictions of these different growth laws during simulated pressure and volume overload, we adjusted the set-points (Table 1) for each growth law such that repeated cycling between baseline end-diastolic and end-systolic stretches induced zero growth.

2.4 Comparison Data: Changes in LV and Myocyte Dimensions Following Overload

Most *in vivo* studies of hypertrophy track left ventricular wall thickness in one or more locations as well as changes in cavity diameter, radius, or circumference. Changes in wall thickness should be analogous to the growth stretches $F_{g,r}$ predicted by the models considered here. Similarly, changes in the left ventricular circumference should be roughly equivalent to $F_{g,f}$ at the midwall, although not necessarily in other layers of the heart wall; note that no commonly reported global dimension is comparable to $F_{g,c}$ predicted by the models. Experimentally, the ratio of LV radius-to-thickness or myocyte length-to-width is frequently used to quantify shape change following growth. Thus, for simulations of both pressure and volume overload for each growth law, the growth ratio was calculated as fiber growth stretch, $F_{g,f}$, divided by radial growth stretch, $F_{g,r}$.

Only some of the acute *in vivo* pressure and volume overload studies used above to quantify changes in stretch also tracked subsequent growth, and those few studies measured growth at very different timepoints. Thus, in order to better determine the levels of expected growth following pressure and volume overload, we included additional studies that quantified LV dimensions. The ratio of LV radius-to-wall thickness decreased during experimental pressure overload and increased during volume overload in dogs (Fig. 2, left column), with considerable variation among the published studies [30–34, 38–41]. Similar trends but even wider ranges were reported in rats (Fig. 2, second column) [2, 7, 42–63]. In order to avoid the confounding effects of failure and decompensation, only studies that reported dimensional changes within 2 to 12 weeks of overload were considered.

There has been considerable evidence showing that changes in myocyte dimensions and shape parallel changes in ventricular dimensions and shape. Myocyte dimensional changes may provide a more relevant local measure of growth for comparison with growth laws that are applied locally, on an element-by-element basis. Thus, we also reviewed studies in which myocyte length and cross-sectional area changes were measured following *in vivo* inducement of pressure or volume overload. Reported myocyte length-to-width ratios increased following volume overload and decreased following pressure overload (Fig. 2, right columns) in both dogs [64, 65] and rats [66–73]. Compared to LV radius-to-wall thickness ratios, myocyte length-to-width ratios changed less in response to overload; the reason for this difference is not clear, particularly given that the rat ventricular and myocyte dimensions were measured at similar times following the onset of overload (mean $\pm$ SEM indicated in Fig. 2). We pooled the dog and rat myocyte dimension measurements for subsequent comparison to the predictions of the various growth models. Tables S1 and S2 provide a comprehensive list of the data plotted in Fig. 2 with associated references.

3 Results

Figure 3A shows the fiber, cross-fiber, and radial growth levels (F_g) predicted by the eight different growth laws in response to prescribed biaxial stretches typical of pressure overload. The range of experimentally reported changes in myocyte width (dashed light green

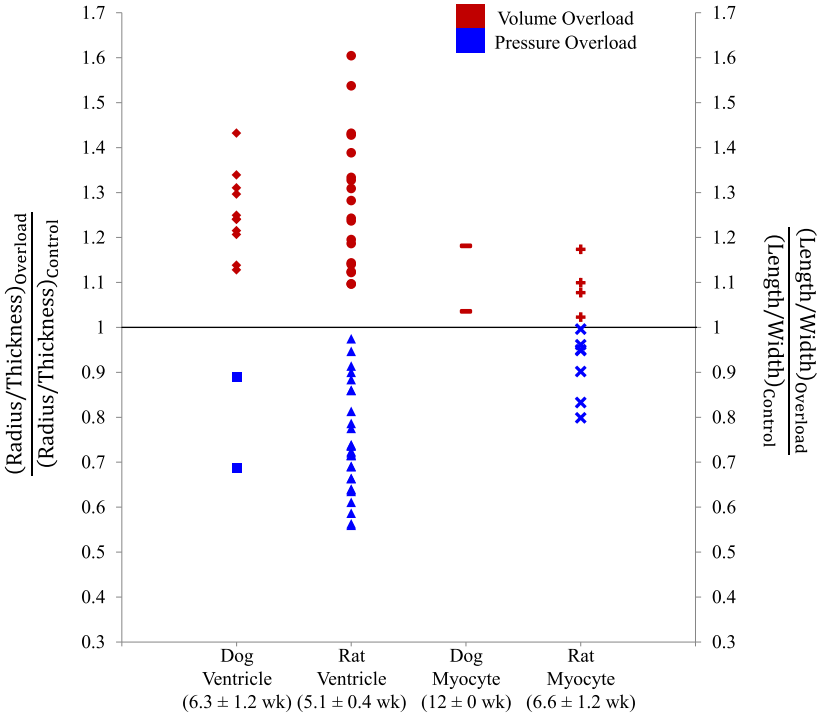

Fig. 2 *Left columns* show reported changes in LV radius-to-wall thickness ratio for *in vivo* studies following the creation of volume and pressure overload in dogs [30–34, 38–41] and rats [2, 7, 42–63], displayed as normalized radius-to wall thickness ratios (*left vertical axis*). *Right columns* show reported changes in myocyte shape for *in vivo* studies following the creation of volume and pressure overload conditions in dogs [64, 65] and rats [66–73], displayed as normalized myocyte length-to-width ratios (*right vertical axis*). The mean ± SEM of the time from onset of overload to dimension measurement is shown below the column labels for each group of studies

lines) and length (dashed dark green lines) following 2 to 12 weeks of pressure overload are shown for comparison. Pressure overload is typically associated with ventricular wall thickening and myocyte width increase *in vivo*. Both KOM and L&T predicted steady-state radial growth within the range of experimentally observed values, while simultaneously predicting realistic levels of steady-state fiber growth. LT2 produced runaway growth in the radial direction. Since LT2 did not reach a steady-state, we halted the pressure overload simulation after two growth time steps, when the predicted fiber-to-radial growth ratio first surpassed the experimental mean; at this growth step, both predicted radial growth and fiber growth were within the range of experimentally observed values. ART also produced runaway growth in the radial and cross-fiber directions; if halted after two growth time steps, when the predicted fiber-to-radial growth ratio first surpassed the experimental mean, predicted radial growth was within the range of experimentally observed values, but the model predicted atrophy in the fiber direction that was inconsistent with experiments. Göktepe et al. [12] created separate laws designed specifically to simulate concentric growth following pressure overload (GCG) and eccentric growth following volume overload (GEG). Similarly to ART, GCG produced maximal growth (limited by the law to $F_{g,r} = 3.0$) in response to prescribed biaxial stretches typical of pressure overload; when halted after growth step 4, when the growth ratio first surpassed the experimental mean, GCG predicted realistic radial

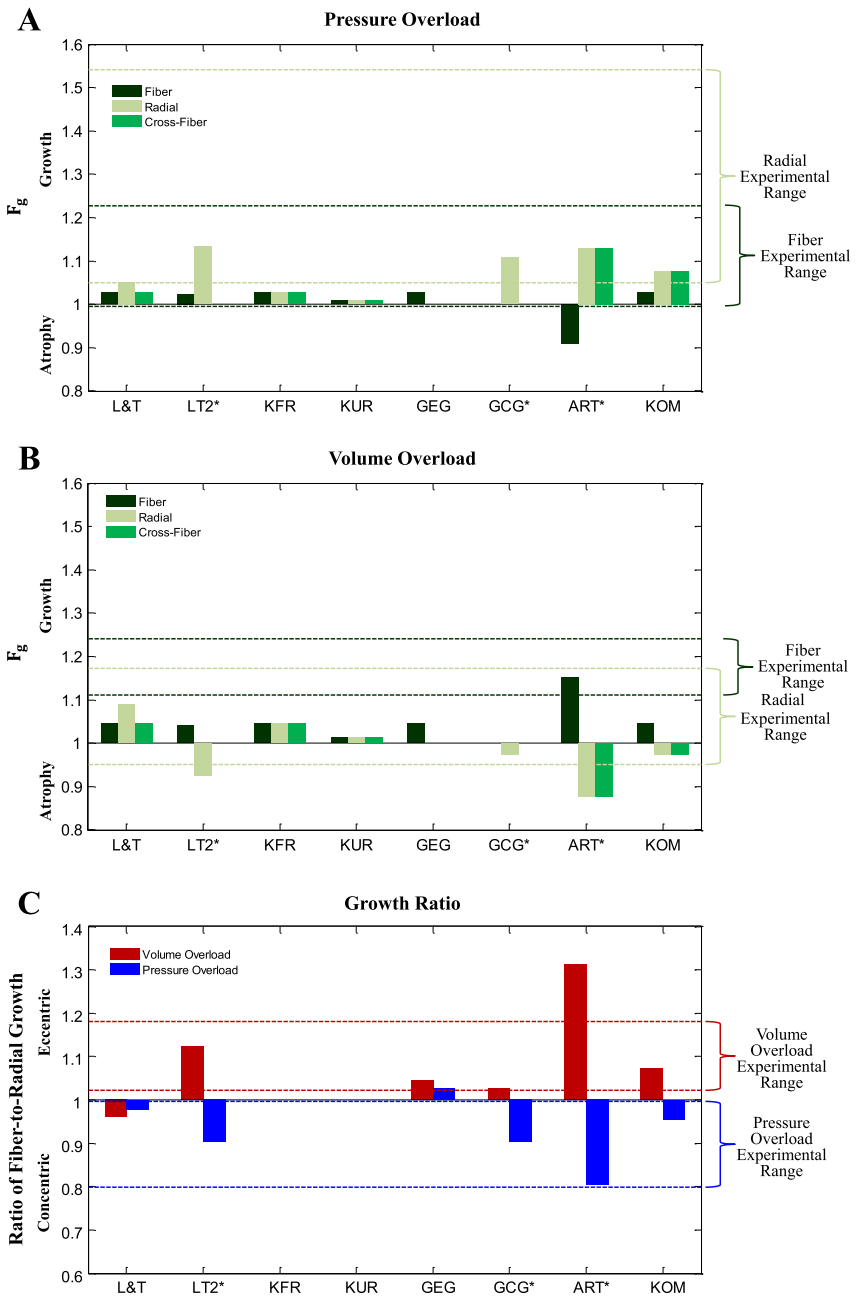

Fig. 3 The fiber, radial, and cross-fiber growth levels (F_g) predicted following pressure (**A**) and volume overload (**B**) by the various growth laws; *green dashed lines* indicate the experimental ranges in myocyte length (*dark green*) and width (*light green*) observed experimentally. (**C**) The fiber-to-radial growth ratio predicted for both pressure and volume overload; *red and blue dashed lines* indicate the experimental ranges for the normalized ratio of myocyte length to width. Three growth laws (GCG, ART, and LT2) predicted runaway growth or atrophy ($F_g > 20$ or $F_g < 0.05$), so simulations were stopped after the time step when the ratio of fiber-to-radial growth first surpassed the value observed experimentally following pressure overload

growth, but by design predicted no fiber or cross-fiber growth. KFR and KUR predicted low levels of isotropic growth that fell outside the experimental range for relative myocyte thickness. By design, GEG was constrained such that there was no growth in the radial or cross-fiber directions and therefore did not produce radial growth in our simulations.

Figure 3B shows the fiber, cross-fiber, and radial growth levels (F_g) predicted by the eight different growth laws in response to prescribed biaxial stretches typical of volume overload. The experimental studies compiled for comparison consistently showed growth in the fiber direction (increased cavity radius and myocyte length), but much more variable changes in ventricular radius and myocyte width. Similarly, most of the growth laws tested (L&T, KFR, GEG, KOM) predicted modest growth in the fiber direction ($\sim 5\%$), with variable responses in the cross-fiber and radial directions ranging from 9% growth (L&T) to 2% atrophy (KOM). ART produced runaway growth, and when halted after two growth time steps (same time point as the pressure overload simulation) yielded fiber growth well within the experimental range but more radial atrophy than observed experimentally. When stopped after 2 growth time steps (same time point as the pressure overload simulation), LT2 predicted more modest fiber growth and substantial radial atrophy. Finally, when stopped after 4 growth time steps (same time point as the pressure overload simulation), GCG produced radial growth within experimental ranges but, by design, no fiber growth.

Figure 3C shows the ratio of fiber growth to radial growth produced by each law in response to prescribed biaxial stretches typical of pressure or volume overload. The ranges of normalized experimental myocyte length-to-width ratios from Fig. 2 are indicated by the blue and red dotted lines, respectively. Consistent with the changes in fiber and radial growth reviewed above, only KOM predicted concentric growth (fiber:radial growth ratio <1) in response to prescribed stretches consistent with experimental pressure overload, predicted eccentric growth (fiber:radial growth ratio >1) in response to prescribed stretches consistent with volume overload, and achieved steady-state. As noted above, the fiber-to-radial growth ratio for the LT2, ART, and GCG simulations using stretches typical of pressure overload fell within the experimental range because this was used as a stopping criterion. At the same growth step, LT2 predicted fiber-to-radial growth ratios near the middle of the experimental range in response to stretch inputs typical of volume overload, while GCG predicted much lower ratios and ART much higher ratios. L&T predicted a steady-state growth ratio within the experimental range for pressure overload, but not volume overload, while GEG captured the trend for volume overload but not pressure overload. Finally, by design KFR and KUR produced isotropic growth with no change in fiber:radial growth ratios. Figure S3 shows the number of growth time steps required for each simulation.

In addition to simulating responses to mean experimentally measured stretches during pressure overload and volume overload, we explored the behavior of each growth law in response to a wide range of end-diastolic and end-systolic stretches. We plotted the predicted ratio of fiber:radial growth for each combination as a contour plot (Fig. 4), and included the experimental stretch ranges (white boxes, Fig. 4A–E) and average myocyte length:width ratios (colored boxes, Fig. 4F) for comparison. Bands of constant predicted growth ratio run diagonally for KOM (Fig. 4A), ART (Fig. 4B), and LT2 (Fig. 4C), reflecting the fact that these laws predict growth based on a combination of end-diastolic and end-systolic stretches or stresses. By contrast, L&T and GEG respond directly to diastolic mechanics (vertical color bands in Figs. 4C–D), while GCG responds to systolic stretch (horizontal color bands in Fig. 4E). Because the *in vivo* stretches computed from experimental pressure and volume overload data differed more in systole than in diastole, only laws that incorporated systolic information were able to match observed trends in fiber:radial growth for both cases.

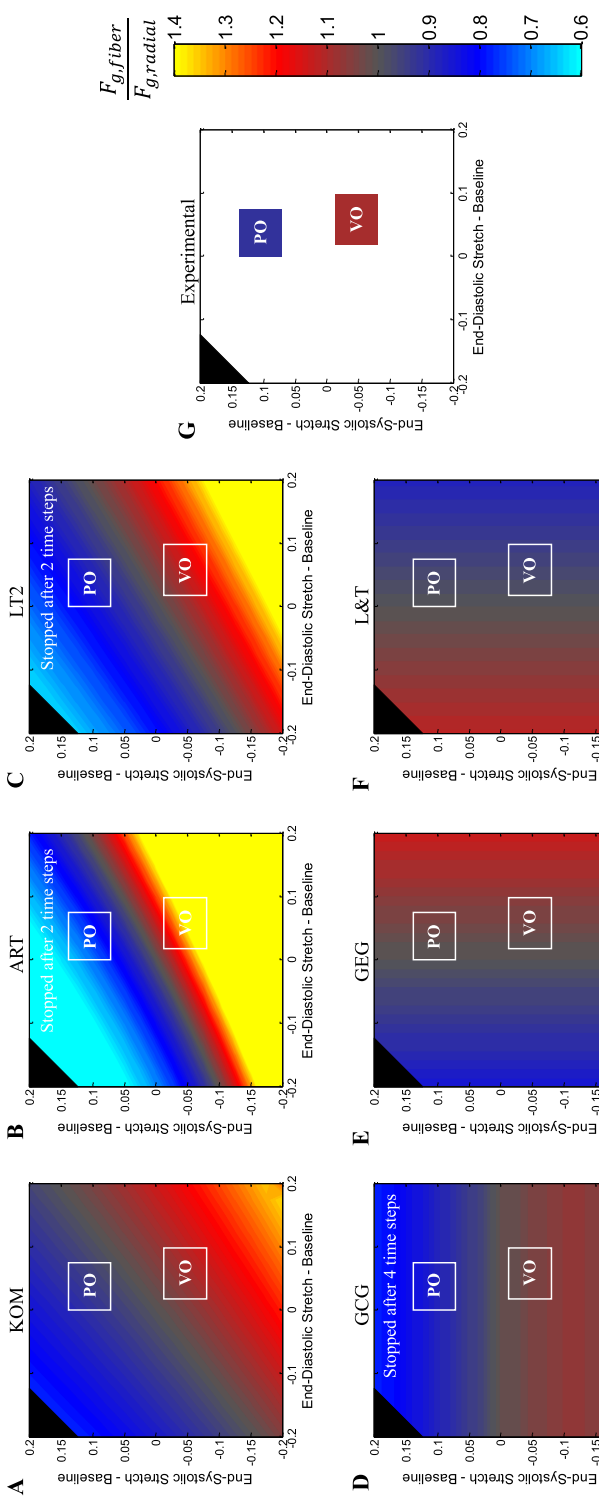

Fig. 4 Predicted fiber-to-radial growth ratios (*color*) given perturbations in end-diastolic (x-axis) and end-systolic stretch (y-axis) for (**A**) KOM, (**B**) ART, (**C**) LT2, (**D**) GCG, (**E**) GEG, and (**F**) L&T. Note that the simulations for ART, LT2, and GCG were stopped after growth time steps 2, 2, and 4, respectively. *White boxes* (**A–F**) indicate the experimental ranges of end-systolic and end-diastolic stretches immediately following pressure and volume overload from Fig. 1B. (**G**) Average myocyte length-to-width ratios following pressure overload and volume overload from Fig. 2 are plotted using the same color scheme as the other panels

4 Discussion

Computational models that correctly predict growth and remodeling of the heart in response to exercise, disease, and various drugs and devices could be very useful in designing new therapies for a range of pathologic conditions. Several groups have now formulated and published equations (often termed "growth laws") that can correctly predict cardiac growth in certain situations. However, to our knowledge no comprehensive comparison of these published growth laws is available to guide researchers and engineers interested in employing models of heart growth in their work. Accordingly, in this study we conducted a systematic comparison of eight published growth laws originally developed to model various experiments that induce growth and remodeling of the heart by surgically altering hemodynamic loading. All of the growth laws tested here were phenomenologic in nature; in other words, they attempted to predict growth from one or more measures of regional mechanics, without representing the complex underlying biology by which those mechanical inputs are transduced in myocytes. They were developed based on the experimental observation that suddenly changing heart mechanics triggers growth [2, 30–34, 38–42], and that the speed or extent of growth appears to correlate with the magnitude of the alteration in mechanics [32, 74, 75].

The growth laws tested here all utilized either myocardial stretches or stresses that were easily computed from stretches and the constitutive parameters provided. Furthermore, they were all originally intended to simulate the response of the LV to experimental pressure overload (an increase in systolic cavity pressure usually induced by constricting the aorta to increase outflow resistance) or volume overload (an increase in cardiac output due to creation of an arteriovenous fistula or mitral regurgitation). Therefore, in order to standardize comparisons in this study, we surveyed the literature to establish a range for the changes in stretch induced by each of these surgical procedures, and simulated the growth response of a section of the LV midwall to these prescribed changes in stretch. We then compared growth predicted by each model to the range of actual growth reported from experimental pressure and volume overload studies.

Most of the published laws reproduced some features of the experiment they were originally designed to simulate—for example, predicting radial growth during pressure overload or growth in the fiber direction during volume overload. However, only three of the laws were able to capture experimentally observed growth patterns in multiple directions at once (Table 2), and only one of these laws produced growth that returned stretches to homeostatic values in our biaxial simulation. As discussed below, these simulations revealed two principles that may prove useful in future cardiac growth models. First, only laws that employed multiple inputs that are poorly coupled during hemodynamic perturbations (such as fiber and crossfiber strain, or end-diastolic and end-systolic stress) were able to capture most of the features of both pressure-overload and volume-overload responses. Second, only laws that used inputs from multiple directions (fiber, cross-fiber, etc.) to drive growth in multiple directions could return to homeostasis following simulated overload in the absence of coupling to a circulatory model.

4.1 Capturing Both Pressure-Overload and Volume-Overload Responses

In many clinically important situations such as myocardial infarction, the changes in mechanics induced in the heart involve some combination of the prototypical changes induced by experimental pressure and volume overload. In such cases a growth model that can correctly predict both the individual pressure and volume overload responses will likely be

Table 2 Summary of growth law predictions in response to pressure and volume overload

Experimental observations		L&T	LT2*	KFR	KUR	GEG	GCG*	ART*	KOM
PO	Radial direction	√	√			●	√	√	√
	Fiber/radial	√	*	●	●	●	*	*	√
	Fiber direction	√	√	√	√	√	√		√
VO	Fiber direction						●	√	
	Fiber/radial	●	√	●	●	√	√	√	√
	Radial direction	√		√	√	√	√		√

√ Predicted value was inside experimental range

* Simulation was halted when predicted value was within experimental range

● Predicted value did not follow experimental trend

required. Of the models tested here, both the KOM and LT2 growth equations were explicitly developed by the authors to capture both overload responses. Therefore, is it not surprising that they captured the key features of both pressure (radial growth stretch >1 and fiber:radial growth ratio <1) and volume (fiber growth stretch and fiber:radial growth ratio both >1) overload in our simulations. However, the ART growth law—originally applied by its authors solely to model pressure overload—also reproduced the key trends. Upon further examination, comparison of these three models with the others offers some potential insight into how to design phenomenologic growth equations to capture multiple responses.

One feature shared by KOM, ART, and LT2 is that all models employed a system of equations involving more than one input. KOM used stretch in two directions (fiber stretch and principal stretch in the plane perpendicular to the fibers) as inputs, while ART and LT2 utilized fiber stretch or stress at two different times during the cardiac cycle (maximum, usually at end diastole, and minimum, usually at end systole). Importantly, each law employed two measures that were weakly correlated with one another in experimental studies of pressure and volume overload (Fig. 5A, D, and G), so that both inputs provided independent information about heart mechanics. By contrast, L&T employed a system of three growth equations involving three different components of the stress tensor, but because all stress components were computed at end-diastole, they were strongly coupled to one another through the constitutive law and did not provide independent information (Fig. 5J). Interestingly, the ranges of experimental data we gathered for this study (Fig. 1B) suggest that it should be possible to capture both pressure and volume overload responses with a single input related to end-systolic fiber stretch: experimentally, pressure and volume overload induced similar changes in diastolic stretch compared to control, but very different changes in systolic stretch (increased in pressure overload, decreased in volume overload). However, most single-input growth laws compared here utilized end-diastolic stretch or stress and therefore predicted similar growth in response to prescribed stretches representing pressure or volume overload (Fig. 4E and F). One law (GCG) did utilize end-systolic stress as its only input, but assumed that growth occurred only in the radial direction, which prevented it from matching experimentally measured volume-overload responses.

4.2 Stopping or Limiting Growth

We had to halt simulations for some of the growth laws compared here after just a few growth time steps in order to prevent runaway growth, while others included explicit limits on the

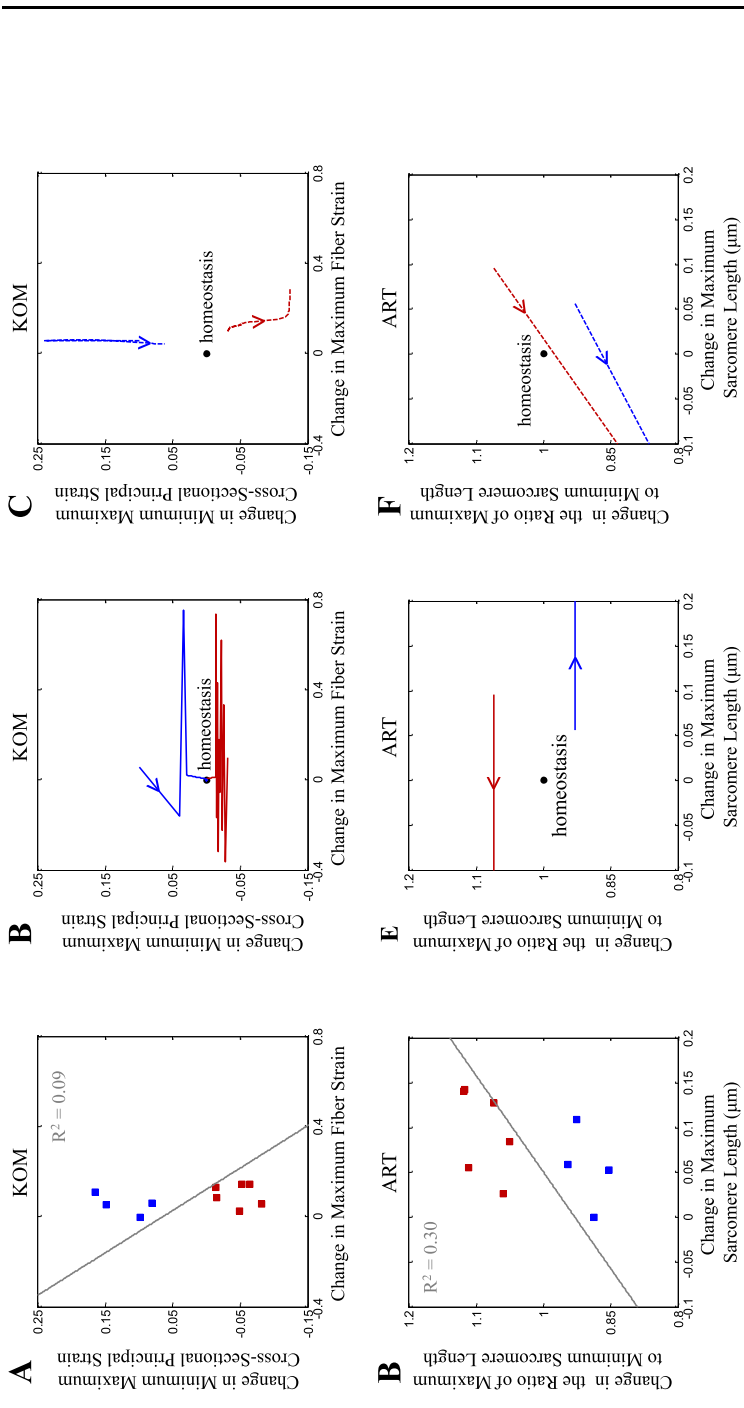

Fig. 5 The correlation of growth stimuli for (**A**) KOM, (**D**) ART, (**G**) LT2, and (**J**) L&T following acute pressure (*blue squares*) and volume overload (*red squares*). Stimulus values were determined from the experimental studies shown in Fig. 2B. Laws utilizing multiple inputs that did not covary strongly across the different experiments were more successful at predicting experimentally measured growth. The evolution of the growth stimuli when overall stretch was prescribed in the fiber and cross-fiber directions for (**B**) KOM, (**E**) ART, (**H**) LT2, and (**K**) L&T. *Arrows* indicate how the stimuli change with increasing growth for both the pressure (*blue*) and volume (*red*) overload simulations. The evolution of the growth stimuli when force was prescribed in the fiber and cross-fiber directions for (**C**) KOM, (**F**) ART, (**I**) LT2, and (**L**) L&T. Again, *arrows* indicate how the stimuli change with increasing growth for both the pressure (*blue*) and volume (*red*) overload simulations

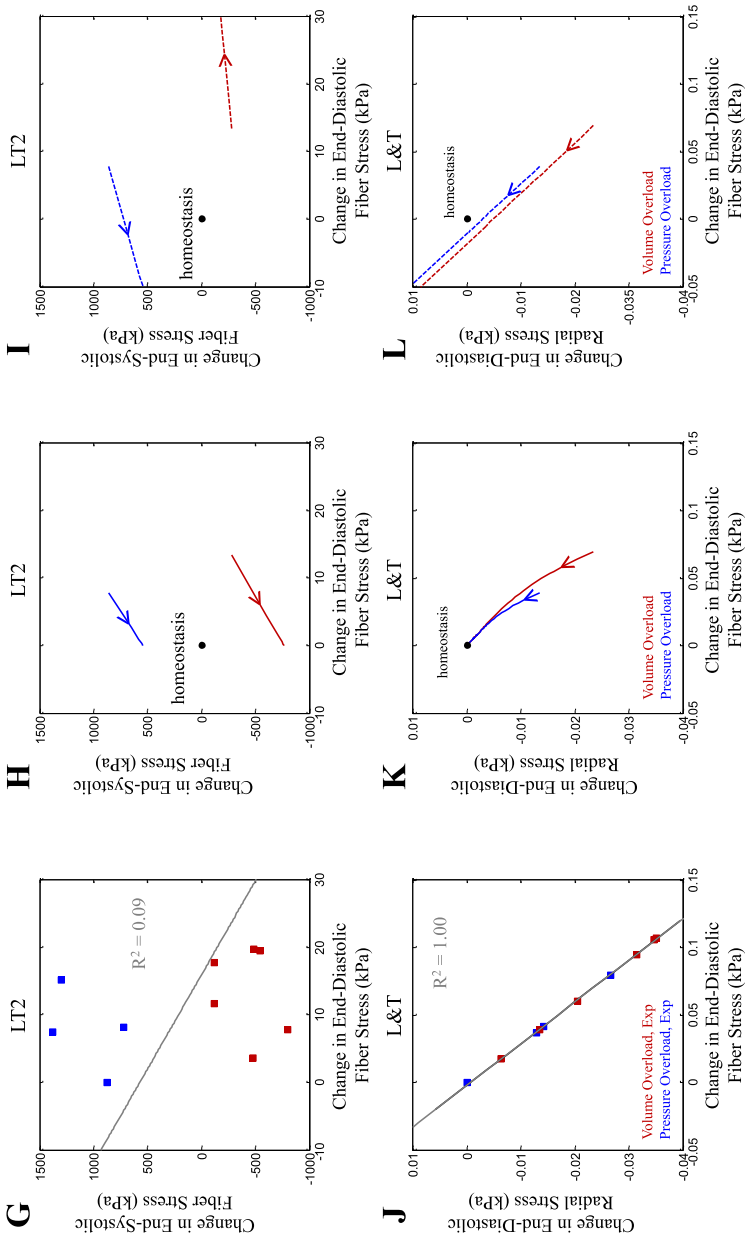

Fig. 5 (*Continued*)

maximum growth allowed. These are two of several approaches that have been employed to prevent growth models from producing experimentally unrealistic magnitudes of growth. One possibility for achieving a stable grown state is if growth normalizes the value of a critical input, returning it to its homeostatic value and thereby preventing additional growth. In the heart, the best-known example of this approach is the (conceptual) model proposed by Grossman et al. [6], where systolic wall stress drives radial growth, and the increase in wall thickness eventually returns wall stress to its homeostatic value.

Our analysis suggests that it is remarkably difficult to devise a growth law that achieves homeostasis following multiple different hemodynamic perturbations (Fig. 5). In Fig. 5B, E, H, and K, we plotted the evolution of the growth stimuli for four of the laws considered here to better visualize how they change as growth proceeds. Only KOM (Fig. 5B) and L&T (Fig. 5K) returned to homeostasis in our prescribed-stretch simulations; these two laws used inputs from two different directions to drive growth in those directions, providing enough degrees of freedom to satisfy two homeostatic conditions simultaneously. For example, in the KOM pressure-overload simulation (blue solid line in Fig. 5B), the increase in prescribed maximum fiber stretch produced growth in the fiber direction, which reduced elastic stretch and returned fiber strain to its homeostatic value; at the same time, elevated cross-fiber strain triggered cross-fiber growth, which reduced cross-fiber strain back to its homeostatic value. (Note that the jagged path is due to oscillation along the sigmoidal stretch-growth curves shown in Figure S1 and could be reduced by re-parameterizing this law for the specific stretch range used here). By contrast, the LT2 law employs two inputs from the same direction, end-diastolic and end-systolic fiber stress. These inputs were nicely decoupled during overload (Fig. 5G), allowing the law to predict different growth trends in response to stretch inputs typical of pressure-overload vs. volume-overload. However, model-predicted growth in the fiber direction (Eq. (4)) reduced diastolic and systolic elastic stretches and stresses proportionally (solid blue line in Fig. 5H), while growth in the radial direction (Eq. (3)) did not affect either input. Thus, under prescribed-stretch boundary conditions, this law was unable to return both stresses to their homeostatic values following perturbation and exhibited runaway growth.

This last example also emphasizes the role of boundary conditions. Many of the original papers describing the growth laws discussed here prescribed diastolic and/or systolic LV pressures typical of control and overload states, then studied how growth evolved in the setting of those applied pressures. In order to represent these boundary conditions in our biaxial simulation, we performed additional simulations in which we cycled between prescribed systolic and diastolic forces rather than between prescribed stretches. Under prescribed-force boundary conditions (Fig. 5I), the LT2 law was again unable to reach homeostasis, but for a different reason: overload altered ED and ES fiber stresses by different fractions of their control values, while subsequent radial growth altered both stresses proportionally. Thus, radial growth could never restore both stresses to their homeostatic values simultaneously. For example, in the pressure-overload simulation, radial thickening reduced both stresses (blue arrow points down and to the right in Fig. 5I), driving ED fiber stress below its setpoint before reaching the ES setpoint (arrow does not pass through the homeostatic point). Interestingly, we note that none of the multi-input growth laws reviewed here returned to homeostasis in prescribed-force simulations. Of course, neither a prescribed-stretch nor a prescribed-force simulation fully replicates the in vivo setting, where hemodynamic adaptations to overload change diastolic and systolic pressures and volumes even as growth proceeds. Furthermore, biologic examples of uncontrolled growth such as progressive dilation leading to heart failure after severe volume overloading suggest that growth may not always return the system to homeostasis.

One final mechanism that might limit growth in response to a mechanical perturbation is if the setpoint gradually resets. In the constrained mixture framework proposed by Humphrey and Rajagopal [76], this occurs as older material is degraded and replaced by new material with a different unstressed reference configuration. In the KUR growth law examined here, the authors achieved something similar by resetting the reference configuration, but this greatly reduced growth. A possible compromise might be a "fading-memory" approach to gradually update the reference configuration with some time lag relative to the current growth time step. One of the models reviewed here (KOM) limited the maximum rate of growth; biologically this might correspond to a maximum rate of new protein synthesis by the myocytes. Other laws reviewed here (GEG and GCG) simply prescribed a maximum level of growth. There has been some speculation that the pericardium could constrain the total amount of LV dilation, but Freeman and LeWinter [77] measured increased pericardial area with heart weight, suggesting that during cardiac hypertrophy the pericardium enlarges as well. At the cellular level, it seems plausible that transport distances could place an upper limit on cell size, but it is currently unclear how or whether transport limits the length, width, or volume of hypertrophying myocytes *in vivo*.

4.3 Limitations and Sources of Error

Many of the limitations of this study arise from the decision to simulate the mechanics of pressure overload and volume overload by applying prescribed stretches to a thin slab of myocardium. All of the growth laws were originally combined with a model of the entire left ventricle (ranging in complexity from compartmental to full finite-element models, Table 1) with a range of boundary conditions that were comparable to our simulations in some cases but not others. The most important difference is that many of the original papers prescribed LV diastolic and/or systolic pressures typical of control and overload states and assumed those pressures did not evolve with growth [9, 11, 12]. The closest analogy in our simple biaxial model would be to cycle between prescribed end-systolic and end-diastolic forces rather than between prescribed diastolic and systolic stretches (Fig. 1C). When we performed these simulations (Fig. 5), all simulations except KUR and GCG showed runaway growth; the reasons for this are discussed in more detail under Stopping or Limiting Growth. In some cases, this result may be due to the fact that our simplified biaxial simulation distorted the feedback of growth on the stimuli that incite it. For example, in a simple cylinder model with circumferentially aligned fibers, circumferential (fiber) growth will increase fiber stresses while radial growth (wall thickening) will decrease them. A prescribed-force biaxial simulation captures the second effect, but not the first. On the other hand, most of the original papers that prescribed pressure boundary conditions in geometrically appropriate LV models also predicted runaway growth unless they stopped their simulations at preset growth levels [11, 12] or employed changing reference configurations [10, 11] to prevent it. In reality, the LV does not operate independently but is connected to the circulation, which reacts and remodels when subjected to overload. Thus, even whole-ventricle models that prescribe LV pressure (stress or force) or stroke volume (strain) do not fully represent the physiology of *in vivo* overload. An alternative approach, utilized by Arts et al. [13], is to couple the LV to an adaptive model of the circulation.

When prescribing stretch profiles to simulate baseline and overload mechanics, we also chose to apply equal stretches in the circumferential and longitudinal directions, based on literature showing that midwall circumferential and longitudinal strains measured during diastolic filling or systolic ejection are approximately equal [16–21]. However, the exact ratio of circumferential to longitudinal stretch obviously varies somewhat with transmural depth,

location within the LV, and with loading. In heart models, this ratio also depends on the overall choice of LV geometry. Thus, we repeated our simulations with a 2:1 ratio of prescribed circumferential to longitudinal stretch and observed no differences in the predictions of most growth laws and only small differences ($\leq$3% change in fiber-radial growth ratios) for KOM and L&T. In no case did the qualitative trend predicted by any law change. These results suggest that the behavior of the growth laws reported here is relatively insensitive to the exact ratio of circumferential to longitudinal stretch prescribed in our simulations. In addition, studies that measured both short-axis and long-axis dimensions in the canine LV immediately following volume [31] or pressure [35] overload found no change in eccentricity (an index of shape), which suggests that overload does not induce major changes in the ratio of circumferential to longitudinal strains *in vivo*. Another limitation of our simulation is that it cannot capture the regional heterogeneity that occurs *in vivo* and can be significant in conditions such as myocardial infarction and dilated heart failure; however, in this respect our study differs less from the original papers proposing these growth laws, most of which assumed axisymmetric geometries and a single growth law and setpoint for the entire LV.

Another potential source of error in our study was estimating the magnitude of end-diastolic stretch relative to the unloaded configuration. We estimated this stretch through extrapolation of segment length data from Fomovsky et al. [25] to 1 mmHg, including in our analysis only data from the six animals where linear fits provided estimates with low variability. For comparison, we also estimated this value using an independent method based on published studies of sarcomere lengths. Rodriguez et al. [78] developed a method to reconstruct sarcomere lengths *in vivo*. They reported the midwall end-diastolic sarcomere length for a single dog as 2.28 μm; comparing this measurement to reported sarcomere length values in unloaded arrested dog hearts of 1.80–1.83 μm by Guccione et al. [79] and 1.9 μm by Spotnitz et al. [80] yields an estimated end-diastolic fiber stretch between 1.20–1.27, a bit lower than our mean value but within the range of the individual values we computed in 6 animals (Figure S2). While we sought to impose physiologically realistic stretches in these experiments, we recognize that they may differ substantially from the stretches computed in the various computational models employed by authors of the original growth laws. We partially accounted for these differences by identifying new setpoints for each law given the control stretches employed here, but could likely obtain a better quantitative match between the predictions of many of these laws and the corresponding myocyte size data if we re-parameterized each law for the specific simulations we performed.

Finally, when considering experimental measurements of growth, we focused on comparisons to myocyte dimensions since growth is a local phenomenon occurring on the myocyte level, even though some of the growth laws were originally validated against changes in LV dimensions. There appears to be a good basis for expecting growth in the fiber direction at the midwall and changes in LV radius or dimension to be congruent, since myocardial fibers at the midwall have been shown to run circumferentially [15]. However, it is less clear how to relate reported changes in myocyte width measured in isolated cells (where the relationship to *in vivo* orientation is lost) or cross-sectional area in histologic sections (includes both radial and cross-fiber components) to changes in LV wall thickness.

Acknowledgements This study was supported by the Hartwell Foundation (CMW) and the National Institutes of Health (U01 HL127654, JWH).

References

1. Anversa, P., Ricci, R., Olivetti, G.: Quantitative structural analysis of the myocardium during physiologic growth and induced cardiac hypertrophy: a review. J. Am. Coll. Cardiol. **7**, 1140–1149 (1986)

2. Cantor, E.J.F., Babick, A.P., Vasanji, Z., Dhalla, N.S., Netticadan, T.: A comparative serial echocardiographic analysis of cardiac structure and function in rats subjected to pressure or volume overload. J. Mol. Cell. Cardiol. **38**, 777–786 (2005)
3. Frey, N., Olson, E.N.: Cardiac hypertrophy: the good, the bad, and the ugly. Annu. Rev. Physiol. **65**, 45–79 (2003)
4. Heineke, J., Molkentin, J.D.: Regulation of cardiac hypertrophy by intracellular signalling pathways. Nat. Rev. Mol. Cell Biol. **7**, 589–600 (2006)
5. Rodriguez, E.K., Hoger, A., McCulloch, A.D.: Stress-dependent finite growth in soft elastic tissues. J. Biomech. **27**, 455–467 (1994)
6. Grossman, W., Jones, D., McLaurin, L.P.: Wall stress and patterns of hypertrophy in the human left ventricle. J. Clin. Invest. **56**, 56–64 (1975)
7. Emery, J.L., Omens, J.H.: Mechanical regulation of myocardial growth during volume-overload hypertrophy in the rat. Am. J. Physiol. **273**, 1198–1204 (1997)
8. Holmes, J.W.: Candidate mechanical stimuli for hypertrophy during volume overload. J. Appl. Physiol. **97**, 1453 (2004)
9. Lin, I.E., Taber, L.A.: A model for stress-induced growth in the developing heart. J. Biomech. Eng. **117**, 343–349 (1995)
10. Taber, L.A.: Biomechanical growth laws for muscle tissue. J. Theor. Biol. **193**, 201–213 (1998)
11. Kroon, W., Delhaas, T., Arts, T., Bovendeerd, P.: Computational modeling of volumetric soft tissue growth: application to the cardiac left ventricle. Biomech. Model. Mechanobiol. **8**, 301–309 (2009)
12. Göktepe, S., Abilez, O.J., Parker, K.K., Kuhl, E.: A multiscale model for eccentric and concentric cardiac growth through sarcomerogenesis. J. Theor. Biol. **265**, 433–442 (2010)
13. Arts, T., Delhaas, T., Bovendeerd, P., Verbeek, X., Prinzen, F.W.: Adaptation to mechanical load determines shape and properties of heart and circulation: the CircAdapt model. Am. J. Physiol., Heart Circ. Physiol. **288**, 1943–1954 (2005)
14. Kerckhoffs, R.C.P., Omens, J.H., McCulloch, A.D.: A single strain-based growth law predicts concentric and eccentric cardiac growth during pressure and volume overload. Mech. Res. Commun. **42**, 40–50 (2012)
15. Streeter, D.D., Spotnitz, H.M., Patel, D.P., Ross, J., Sonnenblick, E.H.: Fiber orientation in the canine left ventricle during diastole and systole. Circ. Res. **24**, 339–347 (1969)
16. Fomovsky, G.M., Holmes, J.W.: Evolution of scar structure, mechanics, and ventricular function after myocardial infarction in the rat. Am. J. Physiol., Heart Circ. Physiol. **298**, 221–228 (2010)
17. Villarreal, F.J., Waldman, L.K., Lew, W.Y.: Technique for measuring regional two-dimensional finite strains in canine left ventricle. Circ. Res. **62**, 711–721 (1988)
18. Lew, W.Y., LeWinter, M.M.: Regional comparison of midwall segment and area shortening in the canine left ventricle. Circ. Res. **58**, 678–691 (1986)
19. Omens, J.H., Farr, D.D., McCulloch, A.D., Waldman, L.K.: Comparison of two techniques for measuring two-dimensional strain in rat left ventricles. Am. J. Physiol. **271**, 1256–1261 (1996)
20. Omens, J.H., MacKenna, D.A., McCulloch, A.D.: Measurement of strain and analysis of stress in resting rat left ventricular myocardium. J. Biomech. **26**, 665–676 (1993)
21. Tobita, K., Schroder, E.A., Tinney, J.P., Garrison, J.B., Keller, B.B.: Regional passive ventricular stress-strain relations during development of altered loads in chick embryo. Am. J. Physiol., Heart Circ. Physiol. **282**, 2386–2396 (2002)
22. Glower, D.D., Spratt, J.A., Snow, N.D., Kabas, J.S., Davis, J.W., Olsen, C.O., Tyson, G.S., Sabiston, D.C., Rankin, J.S.: Linearity of the Frank-Starling relationship in the intact heart: the concept of preload recruitable stroke work. Circulation **71**, 994–1009 (1985)
23. Sodums, M.T., Badke, F.R., Starling, M.R., Little, W.C., O'Rourke, R.A.: Evaluation of left ventricular contractile performance utilizing end-systolic pressure-volume relationships in conscious dogs. Circ. Res. **54**, 731–739 (1984)
24. Rankin, J.S., McHale, P.A., Arentzen, C.E., Ling, D., Greenfield, J.C., Anderson, R.W.: The three-dimensional dynamic geometry of the left ventricle in the conscious dog. Circ. Res. **39**, 304–313 (1976)
25. Fomovsky, G.M., Clark, S.A., Parker, K.M., Ailawadi, G., Holmes, J.W.: Anisotropic reinforcement of acute anteroapical infarcts improves pump function. Circ. Heart Fail. **5**, 515–522 (2012)
26. Omens, J.H., Fung, Y.C.: Residual strain in rat left ventricle. Circ. Res. **66**, 37–45 (1990)
27. Rodriguez, E.K., Omens, J.H., Waldman, L.K., McCulloch, A.D.: Effect of residual stress on transmural sarcomere length distributions in rat left ventricle. Am. J. Physiol. **264**, 1048–1056 (1993)
28. Alyono, D., Ring, W.S., Anderson, M.R., Anderson, R.W.: Left ventricular adaptation to volume overload from large aortocaval fistula. Surgery **96**, 360–367 (1984)
29. Fujisawa, A., Sasayama, S., Takahashi, M., Nakamura, M., Ohyagi, A., Lee, J.D., Yui, Y., Kawai, C.: Enhancement of left ventricular contractility after opening of an arteriovenous fistula in dogs. Cardiovasc. Res. **18**, 51–59 (1984)

30. Nakano, K., Swindle, M.M., Spinale, F., Ishihara, K., Kanazawa, S., Smith, A., Biederman, R.W., Clamp, L., Hamada, Y., Zile, M.R.: Depressed contractile function due to canine mitral regurgitation improves after correction of the volume overload. J. Clin. Invest. **87**, 2077–2086 (1991)
31. Katayama, K., Tajimi, T., Guth, B.D., Matsuzaki, M., Lee, J.-D., Seitelberger, R., Peterson, K.L.: Early diastolic filling dynamics during experimental mitral regurgitation in the conscious dog. Circulation **78**, 390–400 (1988)
32. Kleaveland, J.P., Kussmaul, W.G., Vinciguerra, T., Diters, R., Carabello, B.A.: Volume overload hypertrophy in a closed-chest model of mitral regurgitation. Am. J. Physiol. **254**, 1034–1041 (1988)
33. Carabello, B.A., Nakano, K., Corin, W., Biederman, R., Spann, J.F. Jr.: Left ventricular function in experimental volume overload hypertrophy. Am. J. Physiol. **256**, 974–981 (1989)
34. Sasayama, S., Ross, J., Franklin, D., Bloor, C.M., Bishop, S., Dilley, R.B.: Adaptations of the left ventricle to chronic pressure overload. Circ. Res. **38**, 172–178 (1976)
35. Crozatier, B., Caillet, D., Bical, O.: Left ventricular adaptation to sustained pressure overload in the conscious dog. Circ. Res. **54**, 21–29 (1984)
36. Su, J.B., Crozatier, B.: Preload-induced curvilinearity of left ventricular end-systolic pressure-volume relations. Effects on derived indexes in closed-chest dogs. Circulation **79**, 431–440 (1989)
37. Karunanithi, M.K., Feneley, M.P.: Single-beat determination of preload recruitable stroke work relationship: derivation and evaluation in conscious dogs. J. Am. Coll. Cardiol. **35**, 502–513 (2000)
38. Zile, M.R., Tomita, M., Ishihara, K., Nakano, K., Lindroth, J., Spinale, F., Swindle, M., Carabello, B.A.: Changes in diastolic function during development and correction of chronic LV volume overload produced by mitral regurgitation. Circulation **87**, 1378–1388 (1993)
39. Sabri, A., Rafiq, K., Seqqat, R., Kolpakov, M.A., Dillon, R., Dell'italia, L.J.: Sympathetic activation causes focal adhesion signaling alteration in early compensated volume overload attributable to isolated mitral regurgitation in the dog. Circ. Res. **102**, 1127–1136 (2008)
40. Lee, J.D., Sasayama, S., Kihara, Y., Ohyagi, A., Fujisawa, A., Yui, Y., Kawai, C.: Adaptations of the left ventricle to chronic volume overload induced by mitral regurgitation in conscious dogs. Heart Vessels **1**, 9–15 (1985)
41. Newman, W.H., Webb, J.G.: Adaptation of left ventricle to chronic pressure overload: response to inotropic drugs. Am. J. Physiol. **238**, 134–143 (1980)
42. Wojciechowski, P., Juric, D., Louis, X.L., Thandapilly, S.J., Yu, L., Taylor, C., Netticadan, T.: Resveratrol arrests and regresses the development of pressure overload- but not volume overload-induced cardiac hypertrophy in rats. J. Nutr. **140**, 962–968 (2010)
43. Pawlush, D.G., Moore, R.L., Musch, T.I., Davidson, W.R.: Echocardiographic evaluation of size, function, and mass of normal and hypertrophied rat ventricles. J. Appl. Physiol. **74**, 2598–2605 (1993)
44. Guido, M.C., De Carvalho Frimm, C., Koike, M.K., Cordeiro, F.F., Moretti, A.I.S., Godoy, L.C.: Low coronary driving pressure is associated with subendocardial remodelling and left ventricular dysfunction in aortocaval fistula. Clin. Exp. Pharmacol. Physiol. **34**, 1165–1172 (2007)
45. Melenovsky, V., Benes, J., Skaroupkova, P., Sedmera, D., Strnad, H., Kolar, M., Vlcek, C., Petrak, J., Benes, J., Papousek, F., Oliyarnyk, O., Kazdova, L., Cervenka, L.: Metabolic characterization of volume overload heart failure due to aorto-caval fistula in rats. Mol. Cell. Biochem. **354**, 83–96 (2011)
46. Ryan, T.D., Rothstein, E.C., Aban, I., Tallaj, J.A., Husain, A., Lucchesi, P.A., Dell'Italia, L.J.: Left ventricular eccentric remodeling and matrix loss are mediated by bradykinin and precede cardiomyocyte elongation in rats with volume overload. J. Am. Coll. Cardiol. **49**, 811–821 (2007)
47. Chen, Y.W., Pat, B., Gladden, J.D., Zheng, J., Powell, P., Wei, C.C., Cui, X., Husain, A., Dell'Italia, L.J.: Dynamic molecular and histopathological changes in the extracellular matrix and inflammation in the transition to heart failure in isolated volume overload. Am. J. Physiol., Heart Circ. Physiol. **300**, 2251–2260 (2011)
48. Wilson, K., Guggilam, A., West, T.A., Zhang, X., Trask, A.J., Cismowski, M.J., de Tombe, P., Sadayappan, S., Lucchesi, P.A.: Effects of a myofilament calcium sensitizer on left ventricular systolic and diastolic function in rats with volume overload heart failure. Am. J. Physiol., Heart Circ. Physiol. **307**, 1605–1617 (2014)
49. Gladden, J.D., Zelickson, B.R., Guichard, J.L., Ahmed, M.I., Yancey, D.M., Ballinger, S., Shanmugam, M., Babu, G.J., Johnson, M.S., Darley-Usmar, V., Dell'Italia, L.J.: Xanthine oxidase inhibition preserves left ventricular systolic but not diastolic function in cardiac volume overload. Am. J. Physiol., Heart Circ. Physiol. **305**, 1440–1450 (2013)
50. Wei, C.C., Chen, Y., Powell, L.C., Zheng, J., Shi, K., Bradley, W.E., Powell, P.C., Ahmad, S., Ferrario, C.M., Dell'Italia, L.J.: Cardiac kallikrein-kinin system is upregulated in chronic volume overload and mediates an inflammatory induced collagen loss. PLoS ONE **7**, 1–14 (2012)
51. Miyamoto, M.I., del Monte, F., Schmidt, U., DiSalvo, T.S., Kang, Z.B., Matsui, T., Guerrero, J.L., Gwathmey, J.K., Rosenzweig, A., Hajjar, R.J.: Adenoviral gene transfer of SERCA2a improves left-ventricular function in aortic-banded rats in transition to heart failure. Proc. Natl. Acad. Sci. USA **97**, 793–798 (2000)

52. Litwin, S.E., Katz, S.E., Weinberg, E.O., Lorell, B.H., Aurigemma, G.P., Douglas, P.S.: Serial echocardiographic-Doppler assessment of left ventricular geometry and function in rats with pressure-overload hypertrophy: chronic angiotensin-converting enzyme inhibition attenuates the transition to heart failure. Circulation **91**, 2642–2654 (1995)
53. Kobayashi, S., Yano, M., Kohno, M., Obayashi, M., Hisamatsu, Y., Ryoke, T., Ohkusa, T., Yamakawa, K., Matsuzaki, M.: Influence of aortic impedance on the development of pressure-overload left ventricular hypertrophy in rats. Circulation **94**, 3362–3368 (1996)
54. Hao, J., Kim, C.H., Ha, T.S., Ahn, H.Y.: Epigallocatechin-3 gallate prevents cardiac hypertrophy induced by pressure overload in rats. J. Vet. Sci. **8**, 121 (2007)
55. Doenst, T., Pytel, G., Schrepper, A., Amorim, P., Färber, G., Shingu, Y., Mohr, F.W., Schwarzer, M.: Decreased rates of substrate oxidation ex vivo predict the onset of heart failure and contractile dysfunction in rats with pressure overload. Cardiovasc. Res. **86**, 461–470 (2010)
56. Shyu, K.G., Liou, J.Y., Wang, B.W., Fang, W.J., Chang, H.: Carvedilol prevents cardiac hypertrophy and overexpression of hypoxia-inducible factor-1alpha and vascular endothelial growth factor in pressure-overloaded rat heart. J. Biomed. Sci. **12**, 409–420 (2005)
57. Derumeaux, G., Mulder, P., Richard, V., Chagraoui, A., Nafeh, C., Bauer, F., Henry, J.P., Thuillez, C.: Tissue Doppler imaging differentiates physiological from pathological pressure-overload left ventricular hypertrophy in rats. Circulation **105**, 1602–1608 (2002)
58. Hwang, H.S., Bleske, B.E., Ghannam, M.M.J., Converso, K., Russell, M.W., Hunter, J.C., Boluyt, M.O.: Effects of hawthorn on cardiac remodeling and left ventricular dysfunction after 1 month of pressure overload-induced cardiac hypertrophy in rats. Cardiovasc. Drugs Ther. **22**, 19–28 (2008)
59. Ma, Y., Chen, B., Liu, D., Yang, Y., Xiong, Z., Zeng, J., Dong, Y.: MG132 treatment attenuates cardiac remodeling and dysfunction following aortic banding in rats via the NF-κB/TGFβ1 pathway. Biochem. Pharmacol. **81**, 1228–1236 (2011)
60. Xu, R., Lin, F., Zhang, S., Chen, X., Hu, S., Zheng, Z.: Signal pathways involved in reverse remodeling of the hypertrophic rat heart after pressure unloading. Int. J. Cardiol. **143**, 414–423 (2010)
61. Li, J., Li, P., Feng, X., Li, Z., Hou, R., Han, C., Zhang, Y.: Effects of Losartan on pressure overload-induced cardiac gene expression profiling in rats. Clin. Exp. Pharmacol. Physiol. **30**(11), 827–832 (2003)
62. Kume, O., Takahashi, N., Wakisaka, O., Nagano-Torigoe, Y., Teshima, Y., Nakagawa, M., Yufu, K., Hara, M., Saikawa, T., Yoshimatsu, H.: Pioglitazone attenuates inflammatory atrial fibrosis and vulnerability to atrial fibrillation induced by pressure overload in rats. Heart Rhythm **8**, 278–285 (2011)
63. Phrommintikul, A., Tran, L., Kompa, A., Wang, B., Adrahtas, A., Cantwell, D., Kelly, D.J., Krum, H.: Effects of a Rho kinase inhibitor on pressure overload induced cardiac hypertrophy and associated diastolic dysfunction. Am. J. Physiol., Heart Circ. Physiol. **294**, 1804–1814 (2008)
64. Spinale, F.G., Ishihra, K., Zile, M., DeFryte, G., Crawford, F.A., Carabello, B.A.: Structural basis for changes in left ventricular function and geometry because of chronic mitral regurgitation and after correction of volume overload. J. Thorac. Cardiovasc. Surg. **106**, 1147–1157 (1993)
65. Tsutsui, H., Urabe, Y., Mann, D.L., Tagawa, H., Carabello, B.A., Cooper, G., Zile, M.R.: Effects of chronic mitral regurgitation on diastolic function in isolated cardiocytes. Circ. Res. **72**, 1110–1123 (1993)
66. Gerdes, A.M., Campbell, S.E., Hilbelink, D.R.: Structural remodeling of cardiac myocytes in rats with arteriovenous fistulas. Lab. Invest. **59**, 857–861 (1988)
67. Liu, Z., Hilbelink, D.R., Crockett, W.B., Gerdes, A.M.: Regional changes in hemodynamics and cardiac myocyte size in rats with aortocaval fistulas. 1. Developing and established hypertrophy. Circ. Res. **69**, 52–58 (1991)
68. Gerdes, A.M., Clark, L.C., Capasso, J.M.: Regression of cardiac hypertrophy after closing an aortocaval fistula in rats. Am. J. Physiol. **268**, 2345–2351 (1995)
69. Zierhut, W., Zimmer, H.G., Gerdes, A.M.: Effect of angiotensin converting enzyme inhibition on pressure-induced left ventricular hypertrophy in rats. Circ. Res. **69**, 609–617 (1991)
70. Wang, X., Li, F., Gerdes, A.M.: Chronic pressure overload cardiac hypertrophy and failure in guinea pigs: I. Regional hemodynamics and myocyte remodeling. J. Mol. Cell. Cardiol. **31**, 307–317 (1999)
71. Campbell, S.E., Rakusan, K., Gerdes, A.M.: Change in cardiac myocyte size distribution in aortic-constricted neonatal rats. Basic Res. Cardiol. **84**, 247–258 (1989)
72. Korecky, B., Rakusan, K.: Normal and hypertrophic growth of the rat heart: changes in cell dimensions and number. Am. J. Physiol. **234**, 123–128 (1978)
73. Campbell, S.E., Korecky, B., Rakusan, K.: Remodeling of myocyte dimensions in hypertrophic and atrophic rat hearts. Circ. Res. **68**, 984–996 (1991)
74. Degens, H., Brouwer, K.F.J., Gilde, A.J., Lindhout, M., Willemsen, P.H.M., Janssen, B.J., van der Vusse, G.J., van Bilsen, M.: Cardiac fatty acid metabolism is preserved in the compensated hypertrophic rat heart. Basic Res. Cardiol. **101**, 17–26 (2006)

75. Mohammed, S.F., Storlie, J.R., Oehler, E.A., Bowen, L.A., Korinek, J., Lam, C.S.P., Simari, R.D., Burnett, J.C., Redfield, M.M.: Variable phenotype in murine transverse aortic constriction. Cardiovasc. Pathol. **21**, 188–198 (2012)
76. Humphrey, J.D., Rajagopal, K.R.: A constrained mixture model for growth and remodeling of soft tissues. Math. Models Methods Appl. Sci. **12**, 407–430 (2002)
77. Freeman, G.L., LeWinter, M.M.: Pericardial adaptations during chronic cardiac dilation in dogs. Circ. Res. **54**, 294–300 (1984)
78. Rodriguez, E.K., Hunter, W.C., Royce, M.J., Leppo, M.K., Douglas a, S., Weisman, H.F.: A method to reconstruct myocardial sarcomere lengths and orientations at transmural sites in beating canine hearts. Am. J. Physiol. **263**, 293–306 (1992)
79. Guccione, J.M., O'Dell, W.G., McCulloch, A.D., Hunter, W.C.: Anterior and posterior left ventricular sarcomere lengths behave similarly during ejection. Am. J. Physiol. **272**, 469–477 (1997)
80. Spotnitz, H.M., Sonnenblick, E.H., Spiro, D.: Relation of ultrastructure to function in the intact heart: sarcomere structure relative to pressure volume curves of intact left ventricles of dog and cat. Circ. Res. **18**, 49–66 (1966)